Hindawi
Adsorption Science & Technology
Volume 2022, Article ID 2894099, 19 pages
https://doi.org/10.1155/2022/2894099

Research Article

Selection of Characteristic Particle Size of Drilling Cuttings Based on Adsorption-Desorption Properties: Experiment and Simulation

Shouye Ma

School of Mechatronical Engineering, Beijing Institute of Technology, Beijing 100081, China

Correspondence should be addressed to Shouye Ma; shouye_ma@163.com

Received 2 March 2022; Accepted 27 May 2022; Published 17 June 2022

Academic Editor: S Rangabhashiyam

The direct method for measuring gas content based on image processing, that is, comparing the desorption curves of drilling cuttings with the characteristic particle size with the desorption image in the database to determine the gas content of coal seams, can solve the problems of long measurement time and larger measurement errors of the traditional direct method. However, the precondition to realize this method is to define the characteristic particle size of drilling cuttings. Therefore, this paper performed adsorption and desorption experiments under different particle size ranges and dissimilar adsorption equilibrium pressures, solved the gas migration control equation in coal particles, and determined the characteristic particle size from experimental results and simulation effect. The results showed that gas desorption quantity was positively correlated with adsorption equilibrium pressure, while negatively correlated with the size of a particle size range. The greater the adsorption equilibrium pressure, the better the linear fitting relationship with the maximum desorption quantity, and the maximum correlation coefficient could reach 0.9658. Based on Darcy's law, Langmuir adsorption equation, and mass conservation law, the theoretical control equation of gas migration in coal particles was derived and solved by Open source Field Operation and Manipulation (OpenFOAM). The accuracy of the calculation results of the solver was verified by the derived analytical solution of the gas pressure change of coal particles without considering the adsorption. From the experimental results and simulation results, the characteristic particle size of drilling cuttings was determined to be 0.5-1 mm. The research can provide help for the subsequent development of direct gas content measurement technology based on image processing.

1. Introduction

As the depth and intensity of mining increase, the geological conditions of China's coalfields become more complicated, and the gas content of coal seam increases, which exacerbates the intensity and frequency of gas accidents such as coal and gas outburst [1–4]. Coal and gas outburst is the result of in-situ stress, gas, and coal properties [5–7]. The determination of coal seam gas content before mining is one of the important means to predict coal and gas outburst disasters [8–10]. Among them, the commonly used method is the direct method of determining coalbed gas content in the mine [11, 12], which can be abbreviated as the direct method for short. With the advancement of science and technology, image processing technology is gradually applied to the production of coal mines [13–15]. For instance, Yang et al. [16] measured coal particle size distribution by using digital image process technology. In fact, image processing can also be combined with the direct method to form the dire gas content measurement technology based on image processing. More specifically, the gas content of the measured seam is obtained by collecting the characteristic particle size of the drilling cuttings, measuring the gas desorption curve, using image processing techniques to compare the desorption curve with the images in the database. This method can deal with the problems of long

measurement time and large measurement error of the traditional direct method. However, to implement this technology, the characteristic particle size of drilling cuttings needs to be determined first.

The determination of the characteristic particle size of drilling cuttings can be taken into account in two aspects. The first is the desorption features of coal particles with different particle sizes. Nie et al. [17] conducted isothermal adsorption and desorption experiments of coal particles under dissimilar particle sizes, temperatures, and adsorption equilibrium pressures. According to experimental results, he discovers that the larger the particle size, the greater the initial effective diffusion coefficient, and the smaller the dynamic diffusion coefficient, the smaller the gas desorption rate within the same desorption time. In other words, the smaller the particle size of coal particles, the more gas desorption quantity in the same time, which has been verified in the research of many scholars [18–21]. Liu and Liu [22] investigated the desorption diffusion differences of soft and hard coals under dissimilar particle sizes. They propose that when the particle size decreases to a certain extent, the gas diffusion rate and diffusion coefficient of soft and hard coals are almost the same. And this particle size is referred to as the original particle size. Furthermore, the researchers also deepen the exploration of the desorption features of coal particles with dissimilar particle sizes from the aspects of pressure-bearing [23], mechanical vibration [24], moisture [25], fluid velocity [26], heat and energy [27], multicomponent gas [28], and liquid nitrogen [29].

Secondly, the theoretical control equation of gas migration in coal particles is clarified, and the characteristic particle size of drilling cuttings is determined from the perspective of simulation. Richard [30] believed that the gas migration in coal particles follows Fick's diffusion law and established a classical unipore diffusion model (UDM). Subsequently, Ruckenstein et al. [31] improved on the basis of UDM and create the bidisphere diffusion model (BDM). UDM and BDM have been applied widely in the study of gas desorption features of coal particles [32–34]. However, some scholars also put forward opposite views [35, 36]. Airey [35] proposed that the gas emission of broken coal conforms to Darcy's law. Qin et al. [37, 38] carried out adsorption and desorption experiments of coal particles. It is found that the simulation results of Fick diffusion overlap with the experimental data only at the initial stage of the experiment, while the results of Darcy's seepage model are in good consistent with the experimental data.

In summary, scholars have made fruitful achievements in exploring the desorption features of coal particles with different particle sizes and establishing gas diffusion migration equations. However, few articles combine gas desorption features with equation fitting effects to determine the characteristic particle size of drilling cuttings. The determination of the characteristic particle size can create a prerequisite for the establishment of direct gas content prediction technology based on image processing. Therefore, in this paper, the gas diffusion migration equation was derived and solved by Open source Field Operation and Manipulation (OpenFOAM), and the adsorption and desorption experiments of coal particles under dissimilar particle size ranges and adsorption equilibrium pressures were performed. The characteristic particle size of drilling cuttings was determined from both the experimental results and the simulation effects.

2. Theory and Model

2.1. Theoretical Model of Gas Desorption Process in Coal Particles. The physical essence of the gas desorption process of coal particles is the gas migration in coal particles. To realize a theoretical description of gas migration in coal particles, it is necessary to explore three aspects: the occurrence state of gas in coal particles, the transport law of gas in coal particles, and the abstract structure of coal particles. Based on this, both the adsorbed state and free state gas occurring in coal particles are considered in the process of the theoretical model derivation. Among them, adsorption gas is described by the Langmuir adsorption model, and free gas is approximately regarded as an ideal gas. Moreover, it is believed that gas migration in coal particles obeys Darcy's law of permeability, and the coal particles are treated as a continuous medium.

The assumptions of the theoretical model of coal particles gas desorption process are as follows:

(1) The gas migration in coal particles obeys Darcy's law and the permeability coefficient is a constant

(2) The adsorption process of gas in coal particles satisfies Langmuir isotherm adsorption equation

(3) The gas migration in coal particles is approximately an isothermal process

Based on Darcy's law, the control equation of coal particles gas flowing can be obtained [39]:

$$\vec{u} = -\frac{k}{\mu}\left(\frac{\partial p}{\partial x}\vec{i} + \frac{\partial p}{\partial y}\vec{j} + \frac{\partial p}{\partial z}\vec{k}\right), \tag{1}$$

where $\vec{u}$ is gas velocity (m/s), k expresses permeability of coal particles (m^2), μ indicates gas viscosity coefficient and is 1.71×10^{-5} (MPa·s), and p displays gas pressure in coal particles (MPa).

The gas content of coal particles per volume is $q = q_1 + q_2$. Among them, q_1 reveals free gas quantity (m^3/t); q_2 denotes adsorption gas quantity (m^3/t) and converts all gas quantities to standard state, namely,

$$q_1 = \frac{p}{p_n}\varphi, \tag{2}$$

where p_n is the standard atmospheric pressure (MPa); φ denotes porosity of coal particles and is 10%.

Based on Langmuir adsorption equation, the amount of adsorbed gas quantity of unit volume coal particles can be

obtained [40]:

$$q_2 = \rho \frac{abp}{1+bp}, \tag{3}$$

where ρ expresses coal density (t /m^3); both a and b denote adsorption constants, including a that is 33.5 m^3/t and b that is 0.5979 MPa^{-1}.

According to the law of conservation of mass,

$$\frac{\partial q}{\partial t} = \nabla \cdot \left(\frac{p}{p_n} \vec{u} \right). \tag{4}$$

Joint equation (1) with equation (4) is as follows:

$$\frac{\partial q}{\partial t} = -\frac{k}{2\mu p_n} \Delta\left(p^2\right). \tag{5}$$

Combining equations (2), equation (3), and equation (5), it can be obtained:

$$\frac{\partial((p/p_n)\varphi + \rho(abp/1+bp))}{\partial t} = -\frac{k}{2\mu p_n} \Delta\left(p^2\right). \tag{6}$$

According to the definition of coal seam permeability coefficient, equation (6) can be rewritten as follows:

$$\frac{\partial((p/p_n)\varphi + \rho(abp/1+bp))}{\partial t} = -\lambda \Delta\left(p^2\right). \tag{7}$$

Equation (7) is the theoretical control equation of gas migration in coal particles.

2.2. Solver Design and Coal Particle Geometric Discrete. OpenFOAM can realize the finite volume solution of other partial differential equations except for fluid mechanics. Based on the created partial differential equations, the finite volume method numerical approximation solution of the equation under specific geometric, initial, and boundary conditions is implemented in the OpenFOAM framework. Therefore, applying the basis program library provided by OpenFOAM-6, a solver that can be used to solve equation (7) is designed to explore the migration law of gas in coal particles.

Moreover, PointWise software is applied to construct the geometric dispersion of coal particles. Among them, a uniform unstructured mesh is used for mesh generation, and the mesh density is set to 0.02 mm/dx. Gas in coal particles can be approximately regarded as released into the atmosphere. Therefore, the boundary conditions of spherical coal particles are set as constant pressure boundary conditions, and the pressure is 10^5 MPa. The result of the coal particle geometric discretization model is shown in Figure 1.

2.3. Theoretical Verification of the Solver. The form of equation (7) is too complex to calculate its analytical solution. However, if only the gas seepage process is considered without considering the gas adsorption process in coal particles, equation (7) can be simplified to a great extent, and it is easier to calculate the analytical solution. In order to verify the correctness of the solver designed based on OpenFOAM, the source term in the solver is set to 0 (that is, the adsorption process is ignored). The simulation results under this parameter are compared with the analytical solution of the gas flow equation without considering the adsorption process to verify the correctness of the solver.

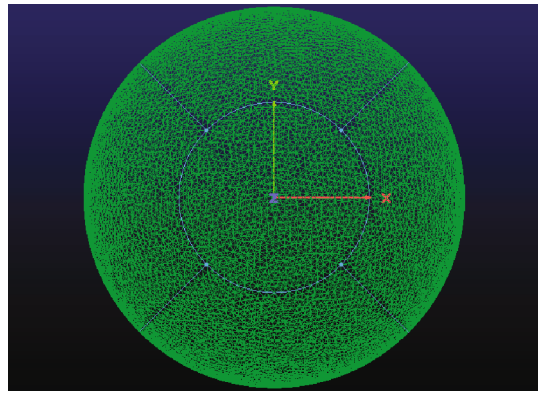

Figure 1: Coal particle geometric discretization model.

The law of mass conservation without considering the adsorption process is as follows:

$$\frac{\partial((p/p_n)\varphi)}{\partial t} = \nabla \cdot \left(\frac{p}{p_n} \vec{u} \right). \tag{8}$$

Combing equation (1) with equation (8),

$$\frac{\partial p}{\partial t} = \frac{k}{\varphi \mu} \left(\frac{2}{r} \frac{\partial p}{\partial r} + \frac{\partial^2 p}{\partial r^2} \right). \tag{9}$$

To solve equation (9), the corresponding initial and boundary conditions must be provided. Assuming that the initial gas pressure outside the coal particles is p_0, the initial condition is shown in equation (10):

$$p(r,t) = p_0. \tag{10}$$

In the process of gas release, the gas pressure outside coal particles can be approximated as atmospheric pressure, and the gas flow velocity at the center point of coal particles is 0, namely, the gas pressure gradient is 0. Thus, the boundary conditions of coal particles can be obtained:

$$\begin{cases} p(r_0,t) = p_n, \\ \dfrac{\partial p(0,t)}{\partial t} = 0. \end{cases} \tag{11}$$

Let $X = pr$, and then equation (10) transforms into the following:

$$\frac{\partial X}{\partial t} = \frac{k}{\varphi \mu} \frac{\partial^2 X}{\partial r^2}. \tag{12}$$

Equation (10) transforms into the following:

$$X(r,0) = p_0 r. \tag{13}$$

Equation (11) transforms into the following:

$$\begin{cases} X(r_0,t) = p_n r_0, \\ X(0,t) = 0. \end{cases} \tag{14}$$

It can be seen that the boundary conditions of the mathematical and physical equations to be solved are inhomogeneous boundary conditions. In order to obtain the analytical solution, it is necessary to transform the inhomogeneous boundary conditions into homogeneous boundary conditions, the transform method as shown in equation (15):

$$X(r,t) = Y(r,t) + Z(r,t). \tag{15}$$

Based on equation (14),

$$Z(r,t) = p_n r. \tag{16}$$

Substitute equation (16) into equation (15):

$$X(r,t) = Y(r,t) + p_n r. \tag{17}$$

Solving the derivative of t for both side of equation (17):

$$\frac{\partial X(r,t)}{\partial t} = \frac{\partial Y(r,t)}{\partial t}. \tag{18}$$

Solving the derivative of r for both side of equation (17):

$$\frac{\partial^2 X(r,t)}{\partial r^2} = \frac{\partial^2 Y(r,t)}{\partial r^2}. \tag{19}$$

Joint equation (12), equation (18), and equation (19) are as follows:

$$\frac{\partial Y(r,t)}{\partial t} = \frac{k}{\varphi\mu}\frac{\partial^2 Y(r,t)}{\partial r^2}. \tag{20}$$

The initial boundary condition of equation (20) is as follows:

$$Y(r,0) = (p_0 - p_n)r. \tag{21}$$

The boundary condition of equation (21) is as follows:

$$\begin{cases} Y(0,t) = 0, \\ Y(r,t) = 0. \end{cases} \tag{22}$$

Solving one integral of t for both sides of equation (19) is as follows:

$$Y(r,t) = \frac{k}{\varphi\mu}\frac{\partial^2 Y(r,t)}{\partial r^2} t + a. \tag{23}$$

Joint equation (20) and equation (23), it can be obtained that $a = (p_0 - p_n)r$.

Solving quadratic integral of r for both sides of equation (20),

$$\left[\left(\frac{[Y(r,t) - (p_0 - p_n)r]\varphi\mu}{tk}\right)r + b\right]r + c = Y(r,t). \tag{24}$$

Joint equation (22) and equation (24), it can be obtained that $b = (p_0 - p_n)\varphi\mu r_0^2/tk$, $c = 0$. Then, equation (24) transforms into:

$$\left[\left(\frac{[Y(r,t) - (p_0 - p_n)r]\varphi\mu}{tk}\right)r + \frac{(p_0 - p_n)\varphi\mu r_0^2}{tk}\right]r = Y(r,t). \tag{25}$$

Deform equation (25) to

$$Y(r,t) = \frac{(p_0 - p_n)r\left(r_0^2 - r^2\right)}{kt/\varphi\mu - r^2}. \tag{26}$$

According to equation (26),

$$X(r,t) = \frac{(p_0 - p_n)r\left(r_0^2 - r^2\right)}{kt/\varphi\mu - r^2} + p_n r. \tag{27}$$

Deform equation (27) to

$$p(r,t) = \frac{(p_0 - p_n)\left(r_0^2 - r^2\right)}{kt/\varphi\mu - r^2} + p_n. \tag{28}$$

In OpenFOAM solver, coal permeability and gas viscosity coefficient are integrated into the permeability coefficient of coal particles. The analytical solution should be consistent with the OpenFOAM solver; so, equation (28) is rewritten as follows:

$$p(r,t) = \frac{(p_0 - p_n)\left(r_0^2 - r^2\right)}{2\lambda p_n t/\varphi - r^2} + p_n \tag{29}$$

Equation (29) was the analytical solution of coal particles gas pressure change without considering adsorption, which was compared with the OpenFOAM numerical solution as shown in Figure 2. Obviously, the numerical solution was in good agreement with the analytical solution, verifying the correctness of the solver based on OpenFOAM to a certain extent.

3. Experimental Devices and Steps

3.1. Experimental Devices. The experimental system of coal particle adsorption and desorption was shown in Figure 3, which was composed of five parts, namely, adsorption and desorption system, gas source control system, vacuum degassing system, constant temperature control system, and data acquisition system. The adsorption and desorption system consisted of a reference tank, an experimental tank,

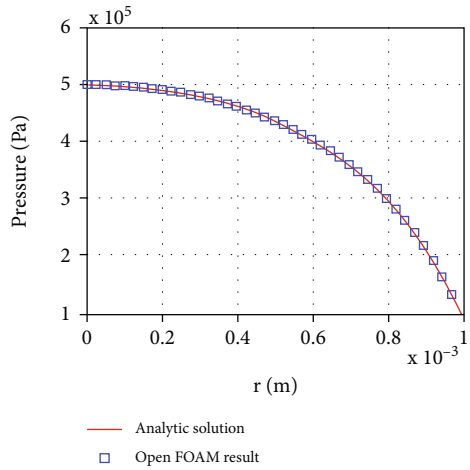

Figure 2: Comparison between numerical solution and analytical solution.

and a gas desorption instrument. The gas desorption instrument was self-developed equipment, operating the principle of drainage and gas gathering. The gas source control system was mainly composed of a high-pressure cylinder and a pressure reducing valve. The methane concentration used in experiments was 99.99%.

A vacuum pump and a vacuum gauge made up the vacuum degassing system. The constant temperature control system included a ribbon heater and a digital thermostat, whose function was to eliminate the influence of environmental temperature change on adsorption and desorption. The data acquisition system consisted of two parts: one was the digital pressure gauge on the experimental tank, and the other was the pressure different sensor in the gas desorption instrument. The range of digital pressure gauge was 0-6 MPa, whose accuracy was 0.05%FS (full scale). The differential pressure sensor had an accuracy of ±0.25%.

3.2. Coal Sample Procurement and Preparation. The coal sample used in experiments was taken from the 2# coal seam in Yangdong Coal, Handan City, Hebei Province, which was a coal seam with the danger of coal and gas outburst. According to the Chinese standard, that is, the coal industrial analysis method (GB/T212-2008), the industrial analysis of experimental coal samples was carried out, and the results were illustrated in Table 1.

Meanwhile, in order to investigate the adsorption and desorption characteristics of coal particles in different particles size ranges, the collected raw coal samples were artificially crushed. Then, coal particles with particle size ranges of 0-0.25 mm, 0.25-0.5 mm, 0.5-1 mm, 1-2 mm, and 2-3 mm were screened by a vibrating screen. After that, the coal particles were put into a drying oven for drying. The drying temperature was 100°C, and the drying time was 12 hours. Finally, the prepared coal particles were weighted with an electronic balance, 50 g as a group, and sealed in a sealed bag for subsequent experiments.

3.3. Experimental Steps. In experiments, six groups of adsorption equilibrium pressures were set, namely, 0.3 MPa, 0.6 MPa, 0.9 MPa, 1.2 MPa, 1.5 MPa, and 1.8 MPa. Combined with five groups of different particle size ranges of coal particles, a total of thirty adsorption and desorption cross experiments were performed. The specific operation process of experiments was as follows:

(1) Preparation work: the preparation 50 g coal particles were placed into the experimental tank, and each equipment was assembled. Then, a certain amount of helium was injected into the experimental system for airtightness detection

(2) Vacuum degassing: the vacuum degassing system was switched on for degassing operations. The degassing lasted for two hours. When the reading on the vacuum gauge showed 50 Pa, it could be determined that the experimental system had approximately reached a vacuum state. After stopping the degassing operation, closed all valves

(3) Inflatable adsorption: the high-pressure cylinder was opened, and a certain amount of methane gas was filled into the reference tank. Once the air pressure in the reference tank had stabilized, the valve between the reference tank and the experimental tank was opened to allow the coal particles to be fully adsorbed. The adsorption time was 12 hours. When the reading of the digital pressure gauge showed the rated adsorption equilibrium pressure and remained unchanged for more than two hours, it could be considered that the coal particles reached the adsorption equilibrium state

(4) Desorption exhaust: when the coal particles reached the adsorption equilibrium state, the valve between the reference tank and the experimental tank was closed. Then, the valve between the experimental tank and the gas desorption instrument was opened for drainage and gas collection. The entire desorption time lasted about two hours

(5) Data processing: the collected experimental data were processed

4. Results and Discussion

4.1. Effect of Adsorption Equilibrium Pressure on Desorption. Based on 30 groups of adsorption and desorption experiments, the typical gas desorption characteristic curves of coal particles under different adsorption equilibrium pressures and dissimilar particle size ranges were obtained, as shown in Figure 4. First of all, from the perspective of a single curve, it was discovered that no matter what the adsorption equilibrium pressure and particle size range were, the variation trend of gas desorption volume in coal particles with desorption time had a certain similarity. In other words, as the desorption time increased, the curve gradually tended to be flat, and its slope decreased bit by bit and finally returned to zero. This indicated that with the extension of

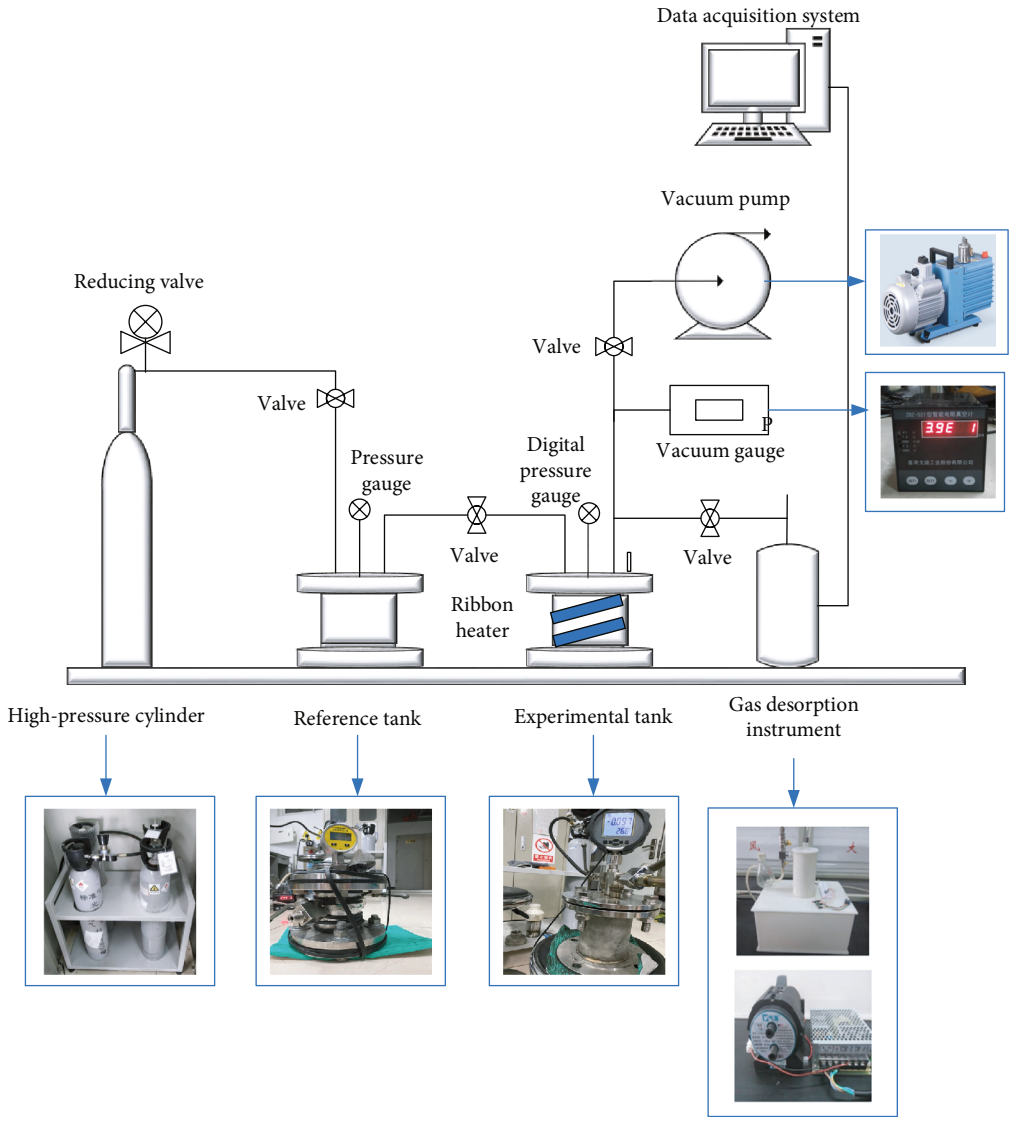

Figure 3: Experimental system diagram.

Table 1: Basic information of coal sample for adsorption and desorption experiments.

Moisture (%)	Ash (%)	Volatile matter (%)	Ture density (t /m^3)	Apparent density (t /m^3)	Porosity (%)
0.81	19.52	18.38	1.56	1.50	3.85

desorption time, the gas desorption rate gradually declined and finally stopped desorption, and the gas desorption volume reached maximum value. Meanwhile, the change rule of a single curve also verified the reliability of those experiments from the side.

Secondary, when the particle size range was kept constant, the gas desorption characteristic curve would change significantly with the variation of adsorption equilibrium pressure, which was not only reflected in the value of curves but also in the shape of curves. Five characteristic curves with a particle size range of 0-0.25 mm were taken as an example for investigating. The curvature of curves added with the increase of adsorption equilibrium pressure. That is, the higher the adsorption equilibrium pressure, the more curved the curve. Simultaneously, under the same time scale, the gas desorption volume value was positively correlated with the adsorption equilibrium pressure, namely, the greater the adsorption equilibrium pressure, the more gas desorption volume. In order to more quantitatively describe the response feature between gas desorption volume and adsorption equilibrium pressure, the desorption volume with a desorption time of 7000 seconds was selected as the maximum desorption volume to explore the correlation between them.

Table 2 and Figure 5 illustrate the variation of gas maximum desorption volume with adsorption equilibrium pressure. Apparently, regardless of particle size ranges, the relationship between maximum desorption volume and adsorption equilibrium pressure showed a similar linear

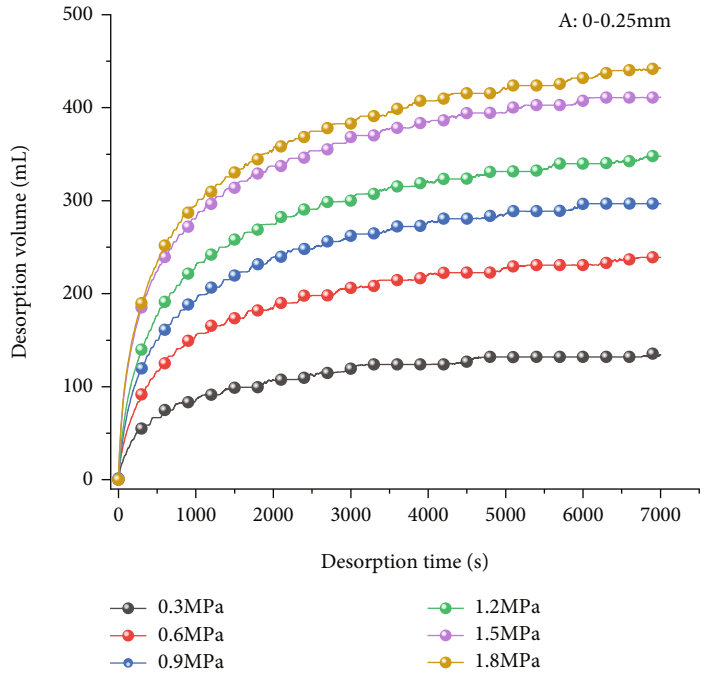

(a)

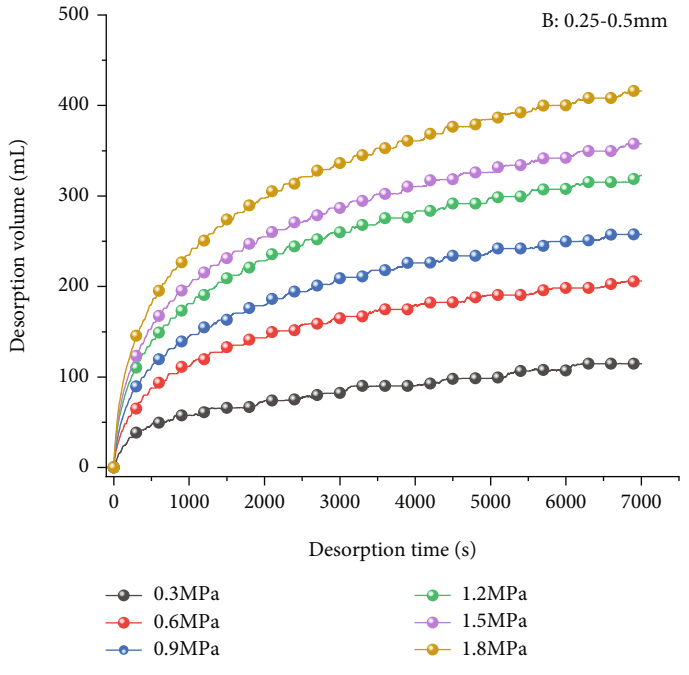

(b)

Figure 4: Continued.

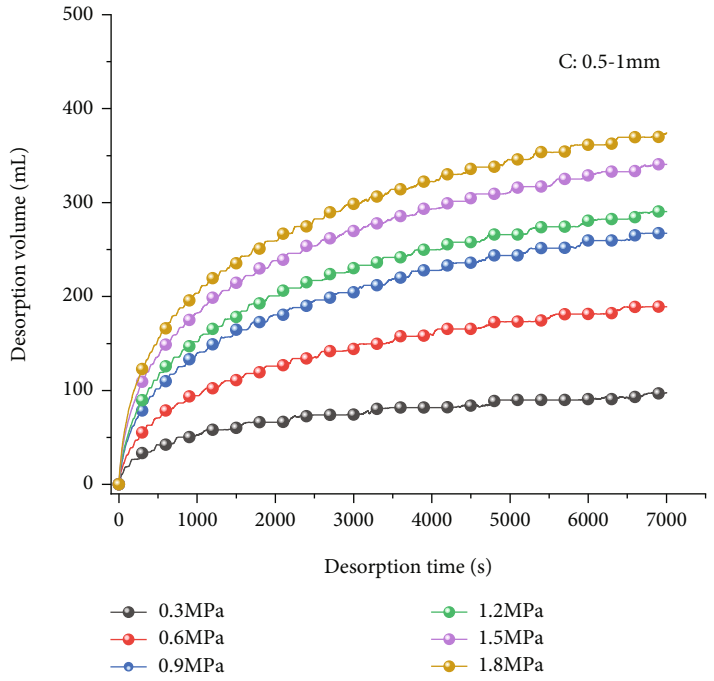

(c)

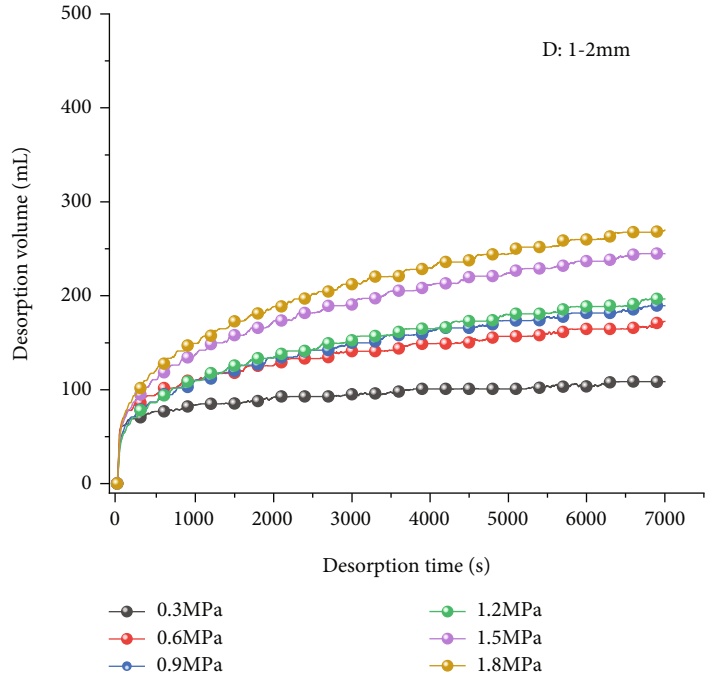

(d)

Figure 4: Continued.

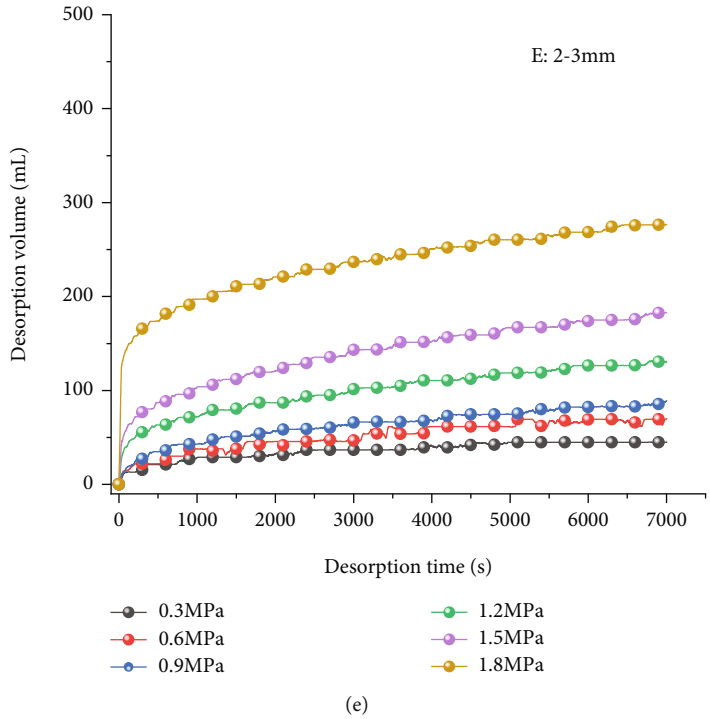

(e)

Figure 4: The trend of desorption volume with time under the same particle size range: (a) 0-0.25 mm, (b) 0.25-0.5 mm, (c) 0.5-1 mm, (d) 1-2 mm, and (e) 2-3 mm.

Table 2: Maximum gas desorption volume under different adsorption equilibrium pressures and particle size ranges (unit: mL).

Range of particle size (mm) Adsorption equilibrium pressure (MPa)	0-0.25	0.25-0.5	0.5-1	1-2	2-3
0.3	134.21	114.73	97.63	108.59	45.00
0.6	238.94	206.31	189.20	172.62	70.00
0.9	296.83	257.62	267.36	189.47	88.95
1.2	347.89	322.88	290.52	196.57	130.78
1.5	411.30	357.62	340.77	244.72	182.89
1.8	442.35	416.04	374.20	269.99	276.56

positive correlation. Moreover, as the particle size range decreased, the linear relationship between them was also obviously enhanced. The particle size range of 0-0.25 mm and the particle size range of 2-3 mm were used as examples, as shown in Figure 6. When the particle size range was 2-3 mm, although there was a linear relationship between maximum desorption volume and adsorption equilibrium pressure, the correlation coefficient between them was only 0.8997. When the particle size range became 0-0.25 mm, the correlation coefficient increased to 0.9658.

Finally, by comprehensively comparing the five figures in Figure 4, it was found that with the increase of particle size range, the variation range of gas desorption volume diminished with the adsorption equilibrium pressure. Likewise, this change was evident in the value of the maximum desorption volume. This phenomenon suggested that the increase of particle size range would weaken the correlation between adsorption equilibrium pressure and gas desorption volume.

4.2. Effect of Particle Size Range on Desorption. Gas desorption volume was not only affected by adsorption equilibrium pressure but also related to particle size ranges. In this section, the influence of particle size range on desorption volume would be researched. Figure 7 shows the variation trend of desorption volume with particle size ranges under different adsorption equilibrium pressures.

No matter how the adsorption equilibrium pressure changed, the trend of desorption volume with particle size range showed certain similarities. Figure 7(b) was taken as an example to illustrate. Firstly, the variation in the particle size range significantly affected the height of the curves, namely, the desorption volume. The smaller the particle size range, the larger the gas desorption volume. A comparison was made between the 2 and 3 mm particle size range and the 0-0.25 mm particle size range. When the desorption time is 7000 seconds, the desorption volume of 2-3 mm coal particle size range was 70 mL, while that of 0-0.25 mm coal particle size range was 238.94 mL, with a difference of more than twice. Secondly, the change in particle size range also had an effect on the shape of the curves. The greater the particle size range, the smoother the curve and the smaller the slope. The curve slope represented the gas desorption rate. In other words, the smaller the particle size range is, the faster the gas desorption rate is in the same time.

By comprehensive comparison of the six diagrams in Figure 7, it could be found that the variation of adsorption

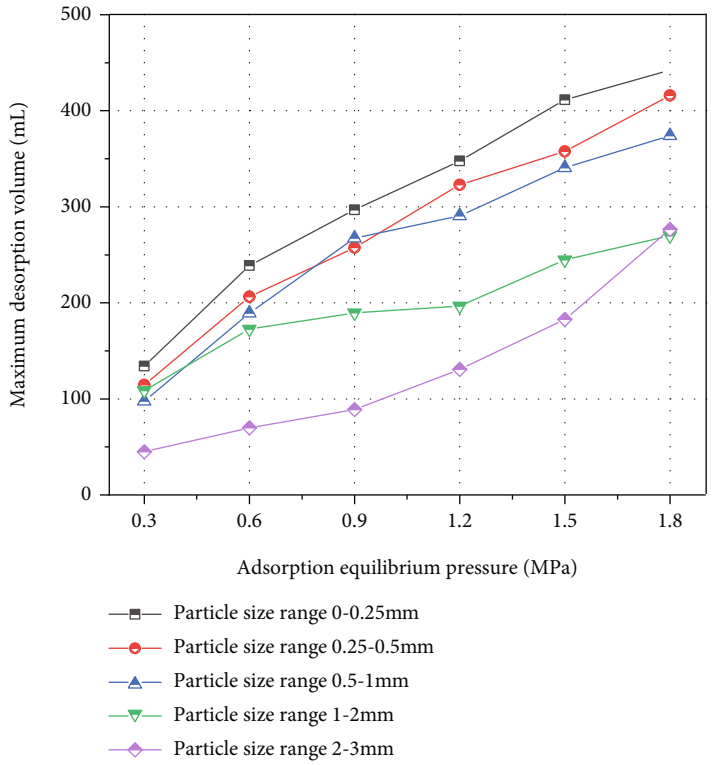

Figure 5: The variation tendency of maximum desorption volume with adsorption equilibrium pressure.

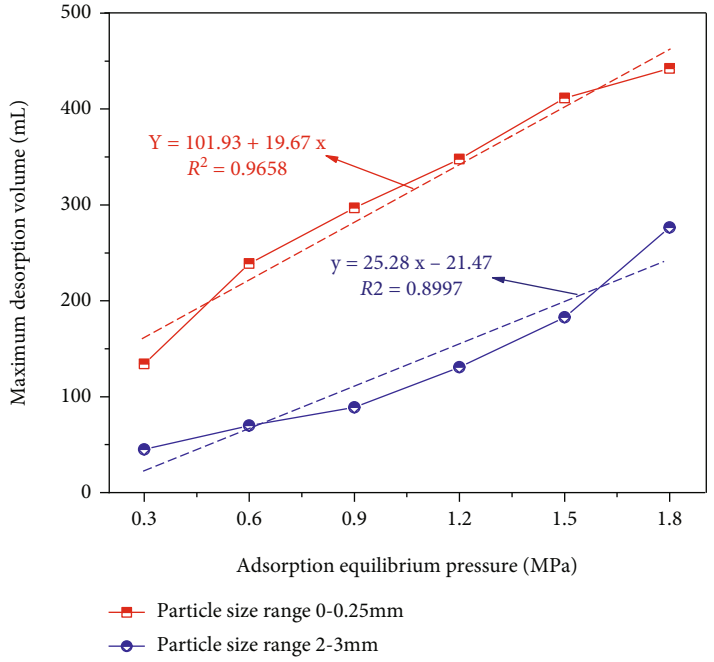

Figure 6: Comparison of linear fitting relationship under different particle size ranges.

equilibrium pressure will remarkably affect the response characteristics between the particle size range and desorption volume of coal particles. Obviously, with the increase of adsorption equilibrium pressure, there were apparent differences between desorption curves under the same particle size range. More specifically, when the desorption time was the same, the curve inclination is higher, and the value is larger. That is to say, in the same time, the greater the gas desorption, the more desorption volume. This indicated that the increase of adsorption equilibrium pressure expanded

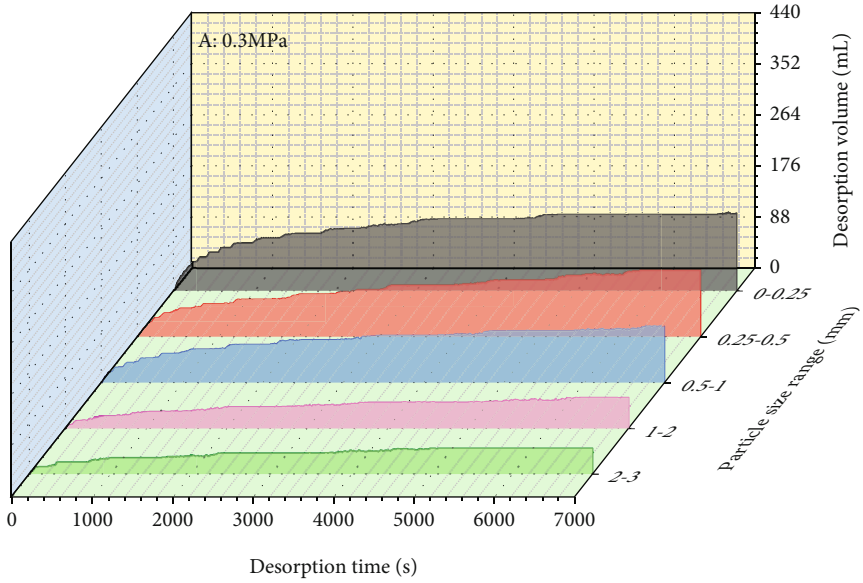

(a)

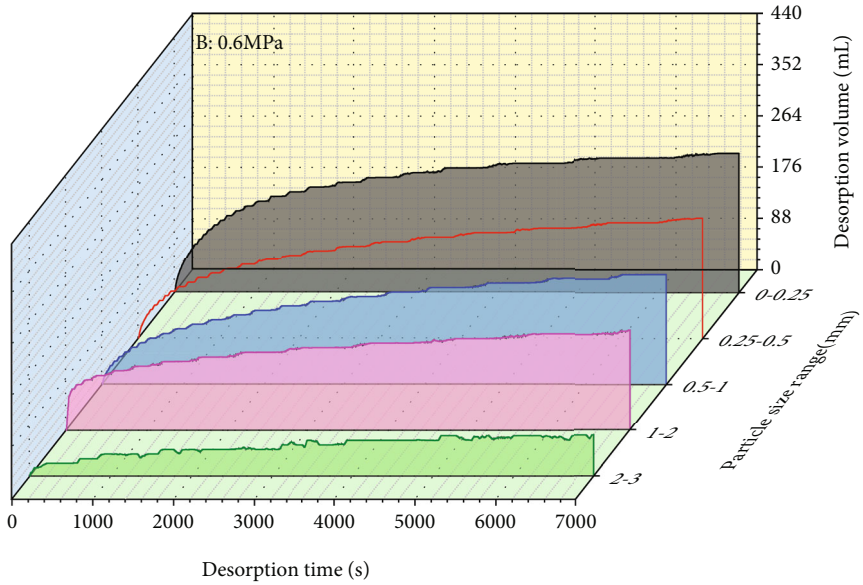

(b)

Figure 7: Continued.

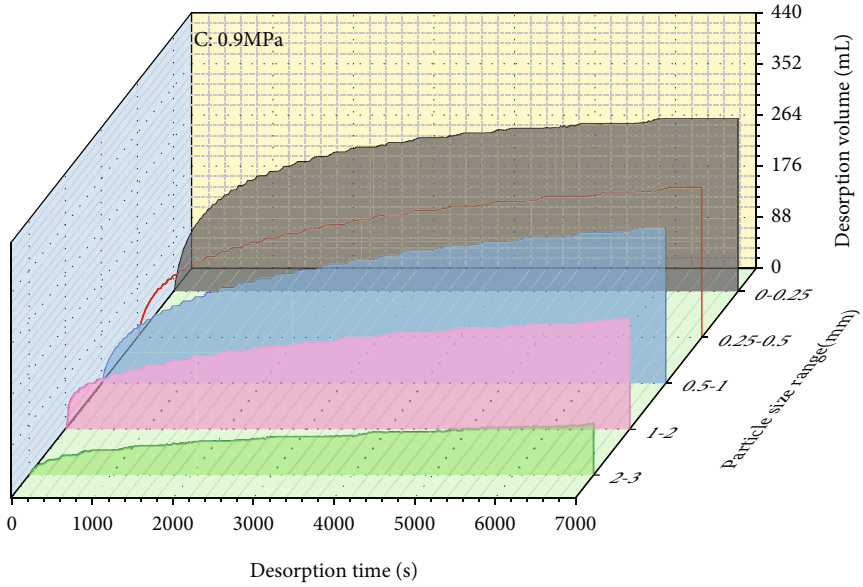

(c)

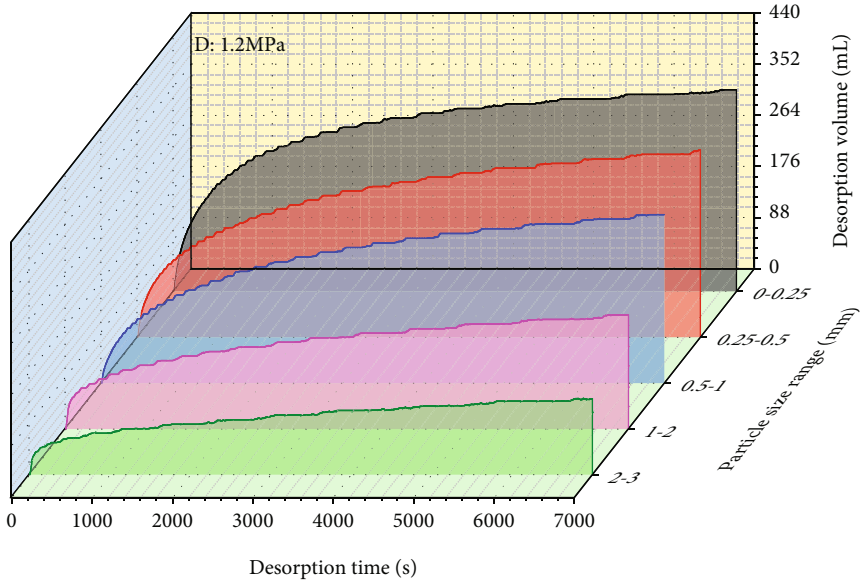

(d)

Figure 7: Continued.

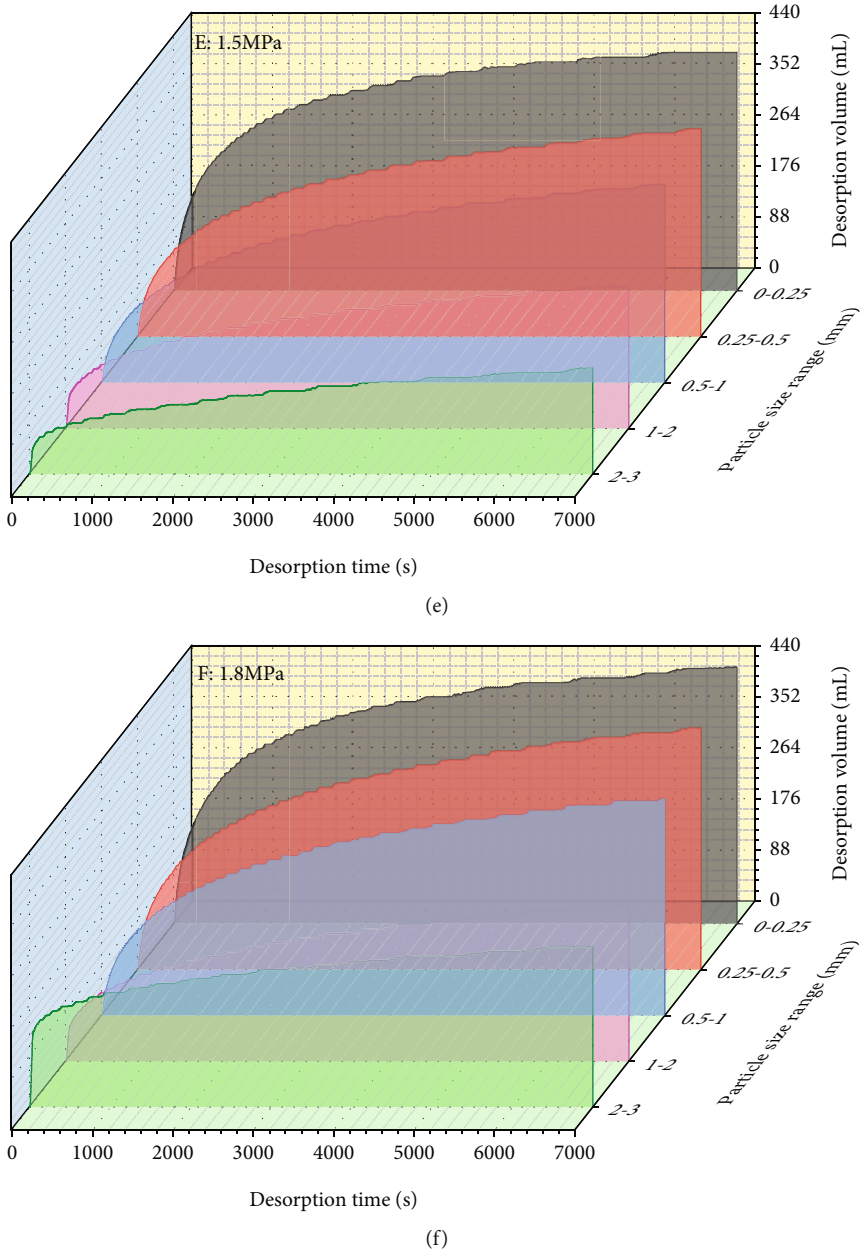

Figure 7: Variation of desorption volume with particle size ranges under different adsorption equilibrium pressures: (a) 0.3 MPa, (b) 0.6 MPa, (c) 0.9 MPa, (d) 1.2 MPa, (e) 1.5 MPa, and (f) 1.8 MPa.

the influence of particle size range on desorption volume. In order to more quantitatively describe the correlation characteristics between particle size range and desorption volume, the gas desorption amount at 7000 seconds was used as an example for analysis, as shown in Figure 8.

Apparently, there was a negative correlation between the maximum desorption volume of coal particles and the particle size range. And also, the difference between them increased with the augment in adsorption equilibrium pressure. When the adsorption equilibrium pressure was 0.3 MPa, the maximum desorption volume of 0-0.25 mm was 134.21 mL, while that of 2-3 mm was 45 mL, with a difference of 89.21 mL. When the adsorption equilibrium pressure was 1.8 MPa, the maximum gas desorption volume was 442.35 mL for the particle size range 0-0.25 mm and 276.56 mL for the particle size range 2-3 mm, a difference of 165.79 mL. Compared with 0.3 MPa, the difference under 1.8 MPa was more evident.

At the same mass and adsorption equilibrium pressure, the gas desorption quantity of coal particles decreased with the increase of particle size range. The reason for this was that the smaller the particle size range of coal particles, the higher the degree of coal fragmentation, the larger the specific surface area of coal particles in contact with the outside world, the more gas adsorbed by the coal matrix, and the shorter the path through which the desorption gas flowed, the faster the desorption speed, and the greater the desorption volume.

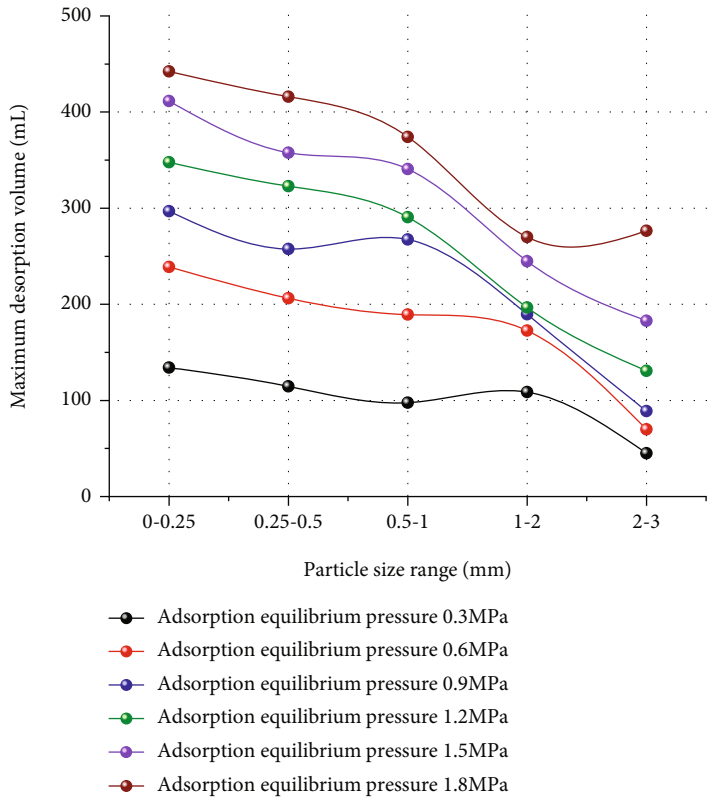

Figure 8: Change trend of maximum desorption volume with particle size range.

If the characteristic particle size of drilling cuttings was considered based on the release capacity of coal particles, the coal particles with the particle size ranges of 1-2 mm and 2-3 mm should be excluded first. Compared with the other three particle size ranges, those desorption volumes are small, and the comparisons of desorption features under dissimilar adsorption equilibrium pressures were less remarkable, which led to them not being regarded as the characteristic particle size of drilling cuttings. For coal particles with particle size ranges of 0-0.25 mm and 0.25-0.5 mm, the desorption volumes were greater under the same scale. However, in practical engineering applications, if the hardness of the coal seam was large, the drilling cuttings of 0-0.25 mm and 0.25-0.5 mm produced in the drilling process were less, which may not collect the rated quality required for desorption experiments. Therefore, it was more appropriate to select 0.5-1 mm particle size range as the characteristic particle size of drilling cuttings. On the one hand, the desorption features of this particle size range are obvious. And on the other hand, it could ensure that enough coal particles were collected in particle work.

4.3. Comparison of Experimental and Simulated Values. According to the analytical solution of gas pressure change without considering the adsorption condition derived in Section 2.3, namely, equation (29), the cumulative gas desorption quantity of coal particles in different particle size ranges under dissimilar adsorption equilibrium pressures could be obtained by using OpenFOAM solver. However, two issues needed to be clarified before proceeding with the simulation.

4.4. Selection of Simulated Coal Particle Size. In experiments, five particle size ranges of 0-0.25 mm, 0.25-0.5 mm, 0.5-1 mm, 1-2 mm, and 2-3 mm were selected for adsorption and desorption experiments. However, the average particle size of coal particles could not be accurately measured on a laboratory scale. Consequently, in OpenFOAM simulation, the intermediate particle size was used as the average particle size to establish the physical model, that is, 0.125 mm particle size to characterize 0-0.25 mm particle size range, 0.375 mm particle size to characterize 0.25-0.5 mm particle size range, and so on.

4.5. Selection of the Simulated Adsorption Equilibrium Pressure. During adsorption and desorption experiments, coal particles first undergo adsorption for eight hours. When the pressure in the experimental tank was kept constant for two hours, desorption was performed. Nevertheless, due to the limitations of experimental conditions and the means of preservation of experimental coal samples, there were certain errors in the measured gas desorption volume in adsorption and desorption experiments. In consequence, it was necessary to determine the accuracy of experimental data. Generally speaking, the larger the adsorption equilibrium pressure, the smaller the error of the measured experimental data. Therefore, in the OpenFOAM solver, the gas desorption quantity of coal particles of various sizes under the adsorption equilibrium pressure of 1.8 MPa was simulated. Meanwhile, the results were compared with the desorption experimental data of coal particles with different particle size ranges to judge coupling between the experimental values and the simulated values, as shown in Figure 9.

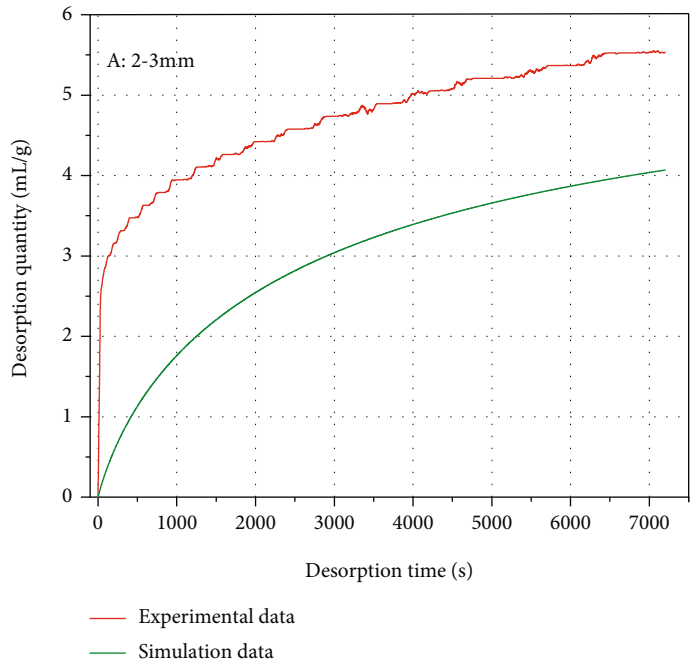

(a)

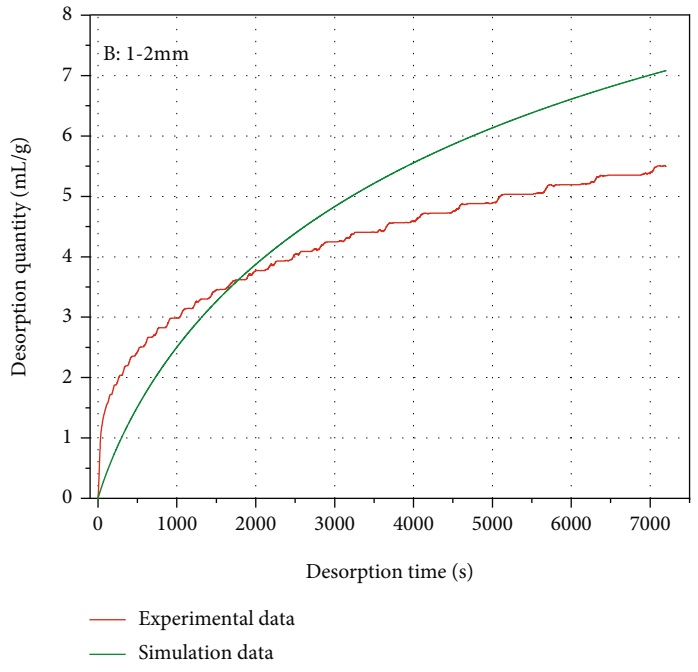

(b)

Figure 9: Continued.

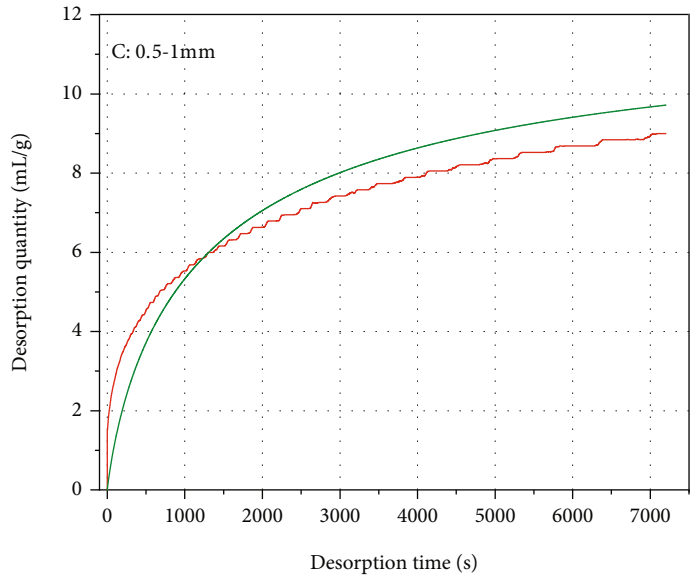

(c)

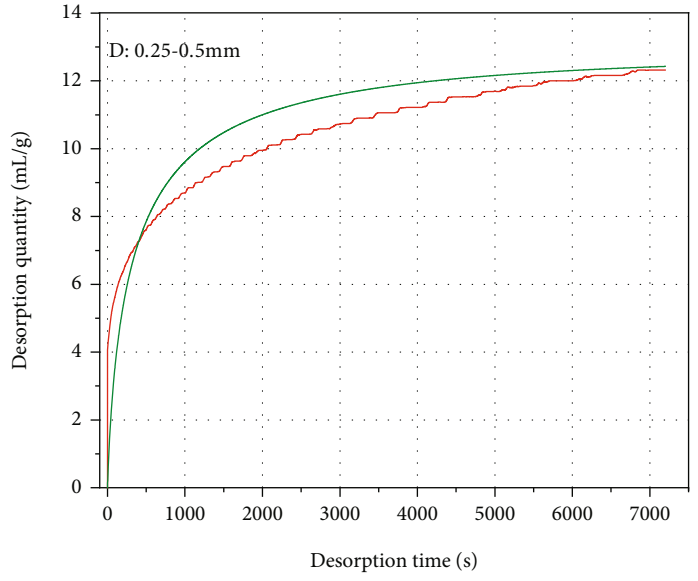

(d)

Figure 9: Continued.

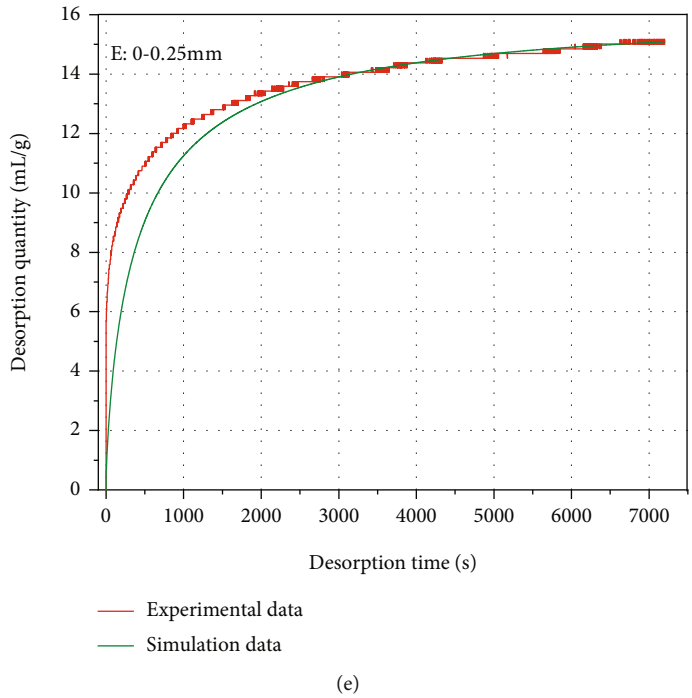

(e)

Figure 9: Comparison of experimental and fitted values under different particle size ranges: (a) 2-3 mm, (b) 1-2 mm, (c) 0.5-1 mm, (d) 0.25-0.5 mm, and (e) 0-0.25 mm.

It could be seen from Figure 9 that the coupling effects between experimental data and simulation data with different particle size ranges were dissimilar. When the particle size range was 2-3 mm, the experimental data was generally greater than the simulation data. However, when the particle size range was 1-2 mm, the corresponding relationship between them changed. Before 1700 seconds, the experimental value was larger than the simulated value, while after 1700 seconds, the simulated value was greater than the experimental value, and the gap between them increased with time. When the particle size range was 0.5-1 mm, the corresponding relationship between them was roughly similar to that of 1-2 mm, whereas there were differences in the equal time and the difference amplitude; that is, the equal time was shortened, and the difference amplitude was reduced. When the particle size range was 0.25-0.5 mm, the time for the simulation data to be equal to the experimental data was further reduced to less than 500 seconds, and the two were almost coincident at 7000 seconds. When the particle size range was 0-0.25 mm, the simulation data and the experimental data had the best agreement, and they almost coincided after 3000 seconds. Those phenomena demonstrated that the smaller the particle size range, the higher the fitting degree between the experimental data and the simulation data, and the better the simulation effect.

The smaller the particle size range of coal particles, the better the fitting effect of the numerical model. The reason for this was mainly due to the choice of particle size for the numerical simulation. As mentioned above, the intermediate particle size was used as the average particle size to establish the physical model. The smaller the particle size range is, the closer the simulated particle size is to the real particle size, and the better the simulation effect is. The larger the particle size range is, the more dispersed the coal particle size distribution is during the experiments. In the simulation, only a constant particle size was selected, so that there would be errors with the actual, and then increases the simulation error. Therefore, the numerical simulation had a certain limitation; that is, it could not accurately simulate the desorption of coal particles with a large particle size range.

When selecting the characteristic particle size of drilling cuttings from the simulation effect, the coal particles with particle size ranges of 1-2 mm and 2-3 mm should be excluded first, because the experimental data of gas desorption in these two particle size ranges were quite different from the simulation data, which was not conducive to subsequent analysis. Secondly, coal particles with particle size ranges of 0-0.25 mm and 0.25-0.5 mm should also be excluded. Although the simulation effects of them were good, due to the small particle size range, sufficient coal particles might not be collected in the actual fieldwork to determine the gas desorption index of coal seam drilling cuttings. Therefore, coal particles with a particle size range of 0.5-1 mm should be selected as the characteristic particle size of drilling cuttings.

From the comprehensive consideration of the desorption characteristics and the fitting effects of the simulated values, the particle size range of 0.5-1 mm was finally determined as the characteristic particle size of drilling cuttings. There were three main reasons for this. To start with, in this particle size range, the desorption features of coal particles were relatively obvious. Secondly, there was a preferable consistency between gas desorption experimental data and simulation data. Finally, this particle size range could ensure that enough coal particles could be collected in engineering

applications for the determination of drilling cuttings desorption index.

5. Conclusion

In this paper, adsorption and desorption experiments of coal particles under different adsorption equilibrium pressures and dissimilar particle size ranges were performed. The theoretical control equation of gas migration in coal particles was derived and calculated by OpenFOAM solver. The characteristic particle size of drilling cuttings was finally determined from experimental results and fitting effects, which laid the foundation for the realization of the direct gas content measurement technology based on image processing. The main conclusions were as follows:

(1) According to Darcy's law, Langmuir adsorption equation, and mass conservation law, the theoretical control equation of gas migration in coal particles was deduced, and the OpenFOAM solver was designed based on the equation. Meanwhile, the accuracy of the calculation results of the solver was verified by the derived analytical solution of coal particles gas pressure change without considering the adsorption situation

(2) The size of coal particle size range was negatively correlated with gas desorption quantity, while the adsorption equilibrium pressure was positively correlated with gas desorption quantity. Moreover, the corresponding relationship between the maximum desorption quantity and adsorption equilibrium pressure was highly consistent with the linear function. Among them, when the adsorption equilibrium pressure was 1.8 MPa, the correlation coefficient of equation fitting reached 0.9658

(3) From the comprehensive consideration of gas desorption features and the degree of fit of the simulation data, the characteristic particle size range of drilling cuttings was finally determined to be 0-0.5 mm. The gas desorption features of this particle size range were evident, the degree of agreement with the simulation data was high, and it could ensure that enough coal particles were collected in practical engineering applications for the subsequent determination of the desorption index of drilling cuttings

In future research, the correctness of selecting 0.5-1 mm particle size range as the characteristic particle size of drilling cuttings could be further verified by researching more adsorption equilibrium pressure states and comparing the particle size distribution characteristics of drilling cuttings under dissimilar destructive actions.

Data Availability

The data used to support the findings of this study are available from the corresponding author upon request.

Conflicts of Interest

The author declares that he/she has no conflicts of interest.

References

[1] H. Y. Liu, B. Y. Zhang, X. L. Li et al., "Research on roof damage mechanism and control technology of gob-side entry retaining under close distance gob," *Engineering Failure Analysis*, vol. 138, p. 106331, 2022.

[2] C. J. Wang, S. Q. Yang, X. W. Li, J. Li, and C. Jiang, "Comparison of the initial gas desorption and gas-release energy characteristics from tectonically-deformed and primary-undeformed coal," *Fuel*, vol. 238, pp. 66–74, 2019.

[3] X. L. Li, Z. Y. Cao, and Y. L. Xu, "Characteristics and trends of coal mine safety development," *Energy Sources Part A: Recovery Utilization And Environmental Effects*, pp. 1–19, 2020.

[4] C. W. Li, Z. Qiao, M. Hao, C. Wei, and G. Li, "The variation of environmental parameters after gas explosion in semi-closed pipeline," *Energy Sources Part A: Recovery Utilization And Environmental Effects*, pp. 1–15, 2021.

[5] X. L. Li, S. J. Chen, and S. Wang, "Study on in situ stress distribution law of the deep mine: taking Linyi Mining area as an example," *Advances In Materials Science And Engineering*, vol. 2021, Article ID 5594181, 2021.

[6] X. L. Li, S. J. Chen, S. M. Liu, and Z. H. Li, "AE waveform characteristics of rock mass under uniaxial loading based on Hilbert-Huang transform," *Journal of Central South University*, vol. 28, no. 6, pp. 1843–1856, 2021.

[7] X. L. Li, S. J. Chen, Q. M. Zhang, and F. Feng, "Research on theory, simulation and measurement of stress behavior under regenerated roof condition," *Geomechanics and engineering*, vol. 26, no. 1, pp. 49–61, 2021.

[8] Z. H. Li, Q. Q. Qi, Y. L. Yang, Y. Zhou, and B. Wang, "Factors impacting gas content measurements using gas desorption by drilling underground boreholes," *Adsorption Science & Technology*, vol. 34, no. 7-8, pp. 488–505, 2016.

[9] L. Wang, L. B. Cheng, Y. P. Cheng et al., "A new method for accurate and rapid measurement of underground coal seam gas content," *Journal of Natural Gas Science and Engineering*, vol. 26, pp. 1388–1398, 2015.

[10] S. Xue and L. Yuan, "The use of coal cuttings from underground boreholes to determine gas content of coal with direct desorption method," *International Journal of Coal Geology*, vol. 174, pp. 1–7, 2017.

[11] G. Q. Yan, G. Wang, L. Xin, W. Du, and Q. Huang, "Direct fitting measurement of gas content in coalbed and selection of reasonable sampling time," *International Journal of Mining Science and Technology*, vol. 27, no. 2, pp. 299–305, 2017.

[12] Y. W. Liu, Y. Du, Z. Q. Li et al., "A rapid and accurate direct measurement method of underground coal seam gas content based on dynamic diffusion theory," *International Journal of Mining Science and Technology*, vol. 30, no. 6, pp. 799–810, 2020.

[13] J. Busse, J. R. de Dreuzy, S. G. Torres, D. Bringemeier, and A. Scheuermann, "Image processing based characterisation of coal cleat networks," *International Journal of Coal Geology*, vol. 169, pp. 1–21, 2017.

[14] C. M. Sun, S. G. Gao, and Y. Li, "Mesomechanics coal experiment and an elastic-brittle damage model based on texture features," *International Journal of Mining Science and Technology*, vol. 28, no. 4, pp. 639–647, 2018.

[15] J. Perkins, O. Williams, T. Wu, and E. Lester, "Automated image analysis techniques to characterise pulverised coal particles and predict combustion char morphology," *Fuel*, vol. 259, article 116022, 2020.

[16] X. H. Yang, T. Ren, and L. H. Tan, "Size distribution measurement of coal fragments using digital imaging processing," *Measurement*, vol. 160, article 107867, 2020.

[17] B. S. Nie, T. Yang, X. C. Li, L. Li, and H. Lu, "Research on diffusion of methane in coal particles," *Journal of China university of mining & technology*, vol. 42, no. 6, pp. 975–981, 2013.

[18] J. L. Soares, A. L. B. Oberziner, H. J. Jose, A. E. Rodrigues, and R. F. Moreira, "Carbon dioxide adsorption in Brazilian coals," *Energy & Fuels*, vol. 21, no. 1, pp. 209–215, 2007.

[19] M. Lutynski and M. A. G. Gonzales, "Characteristics of carbon dioxide sorption in coal and gas shale - the effect of particle size," *Journal natural gas science & engineering*, vol. 28, pp. 558–565, 2016.

[20] E. T. Chen, L. Wang, Y. P. Cheng et al., "Pulverization characteristics of coal affected by magmatic intrusion and analysis of the abnormal gas desorption index on drill cuttings," *Adsorption Science & Technology*, vol. 36, no. 1-2, pp. 805–829, 2018.

[21] T. Gao, D. Zhao, C. Wang, and Z. C. Feng, "Energy variation in coal samples with different particle sizes in the process of adsorption and desorption," *Journal of Petroleum Science and Engineering*, vol. 188, article 106932, 2020.

[22] Y. W. Liu and M. J. Liu, "Effect of particle size on difference of gas desorption and diffusion between soft coal and hard coal," *Journal of China Coal Society*, vol. 40, no. 3, pp. 579–587, 2015.

[23] C. W. Li, H. L. Xue, and W. B. Liu, "Experimental study on gas diffusion in coal under stress," *Journal of China Coal Society*, vol. 43, no. 3, pp. 717–723, 2018.

[24] X. X. Chen, L. Zhang, and M. L. Shen, "Experimental research on desorption characteristics of gas-bearing coal subjected to mechanical vibration," *Energy Exploration & Exploitation*, vol. 38, no. 5, pp. 1454–1466, 2020.

[25] D. Zhao, C. Zhang, H. Chen, and Z. C. Feng, "Experimental study on gas desorption characteristics for different coal particle sizes and adsorption pressures under the action of pressured water and superheated steam," *Journal of Petroleum Science and Engineering*, vol. 179, pp. 948–957, 2019.

[26] S. Tao, D. Z. Tang, H. Xu et al., "Fluid velocity sensitivity of coal reservoir and its effect on coalbed methane well productivity: a case of Baode Block, northeastern Ordos Basin, China," *Journal of Petroleum Science and Engineering*, vol. 152, pp. 229–237, 2017.

[27] J. C. Ye, S. Tao, S. P. Zhao, S. Li, S. Chen, and Y. Cui, "Characteristics of methane adsorption/desorption heat and energy with respect to coal rank," *Journal of Natural Gas Science and Engineering*, vol. 99, article 104445, 2022.

[28] X. J. Qin, H. Singh, and J. C. Cai, "Sorption characteristics in coal and shale: a review for enhanced methane recovery," *Capillarity*, vol. 5, no. 1, pp. 1–11, 2022.

[29] S. M. Liu, X. L. Li, D. K. Wang, and D. Zhang, "Investigations on the mechanism of the microstructural evolution of different coal ranks under liquid nitrogen cold soaking," *Energy Sources Part A: Recovery Utilization And Environmental Effects*, pp. 1–17, 2020.

[30] M. B. Richard, *Diffusion in and through Solids*, Cambridge University Press, 1951.

[31] E. Ruckenstein, A. S. Vaidyanathan, and G. R. Youngquist, "Sorption by solids with bidisperse pore structures," *Chemical Engineering Science*, vol. 26, no. 9, pp. 1305–1318, 1971.

[32] A. Busch and Y. Gensterblum, "CBM and CO2-ECBM related sorption processes in coal: a review," *International Journal of Coal Geology*, vol. 87, no. 2, pp. 49–71, 2011.

[33] S. B. Hu, X. C. Li, and E. Y. Wang, "Experimental and numerical study on scale effects of gas emission from coal particles," *Transport in Porous Media*, vol. 114, no. 1, pp. 133–147, 2016.

[34] C. W. Li, Z. Qiao, M. Hao, Y. Wang, and B. Han, "Gas desorption diffusion behavior in coal particles under constant volume conditions: experimental research and model development," *Energy Sources Part A: Recovery Utilization and Environmental Effects*, vol. 44, no. 1, pp. 1566–1582, 2022.

[35] E. M. Airey, "Gas emission from broken coal. An experimental and theoretical investigation," *International Journal Rock Mechanics And Mining Science*, vol. 5, no. 6, pp. 475–494, 1968.

[36] W. Liu, C. He, Y. P. Qin, and P. Liu, "Inversion of gas permeability coefficient of coal particle based on Darcy's permeation model," *Journal of Natural Gas Science and Engineering*, vol. 50, pp. 240–249, 2018.

[37] Y. P. Qin, Y. J. Hao, P. Liu, and J. Wang, "Coal particle gas desorption experiment and numerical simulation in enclosed space," *Journal of China Coal Society*, vol. 40, no. 1, pp. 87–92, 2015.

[38] Y. P. Qin, C. X. Wang, J. Wang, and X. B. Yang, "Mathematical model of gas emission in coal particles and the numerical solution," *Journal of China Coal Society*, vol. 37, no. 9, pp. 1466–1471, 2012.

[39] Y. Lou, H. Q. Song, and J. S. Yang, "Productivity equation of fractured well in CBM reservoirs," *Journal of Natural Gas Science and Engineering*, vol. 11, pp. 39–45, 2013.

[40] G. W. Lu, C. T. Wei, J. L. Wang, G. Yan, J. Zhang, and Y. Song, "Methane adsorption characteristics and adsorption model applicability of tectonically deformed coals in the Huaibei coalfield," *Energy and Fuel*, vol. 32, no. 7, pp. 7485–7496, 2018.